Analytical PM Eddy Currents Loss Evaluations in Inverter-Fed Slotless Machines Induced by SVM Control Using Polar Coordinates Formulations

Matteo Leandro, *Student Member, IEEE,* and Jonas Kristiansen Nøland, *Senior Member, IEEE*

***Abstract*—Space vector modulation (SVM) is a widespread method for controlling PM machines. However, the switching harmonics contribute to eddy current losses in the magnet region. In the analytical modeling of slotless PM machines, the inverter model is reduced to overlook the actual modulation and neglects many higher-order harmonics. This is the first time the full implementation of an experimentally validated analytical SVM has been applied to analytical PM eddy current loss evaluations. The inverter model operates synergically with previously developed analytical field formulations. We show that the inverter's output current from SVM control can be conveniently post-processed to be suitable for analytical implementation. Major numerical implementation challenges are highlighted and addressed for the first time. Our work shows a considerable improvement in the precision both when including and excluding the eddy currents reaction field. Nevertheless, the models' limitations are also emphasized. Finally, the code implementation of the models is made available in the reference list, yielding full reproducibility.**

***Index Terms*—Analytical method, eddy current losses, inverter-fed machine, slotless machine.**

NOMENCLATURE

δ	Inverse skin depth $[1/\mathrm{m}]$
κ	Net zero current density term, $[\mathrm{A/m^2}]$
λ	Lanczos correction factor $[-]$
$\mathbb{J}_m$, $\mathbb{Y}_m$	1st & 2nd kind Bessel functions of order m $[-]$
n_s	Mechanical speed, [rpm] or [pu]
μ_0	Vacuum air permeability, $4\pi \cdot 10^{-7}$ H/m
μ_r	Relative permeability of magnets, $[-]$
ω_r, ω	Mechanical & electrical ang. frequency, $[\mathrm{rad/s}]$
$\Re_s$	Per phase armature resistance, $[\Omega]$ or [pu]
σ, σ_{pm}	Generic & magnet conductivity, $[\mathrm{S/m}]$
τ_m	Mechanical torque, [Nm] or [pu]
φ_n, α	Time harmonic angle & stator ang. coord. [rad]
ϑ	Angular coordinate position, [rad]
ξ_{pm}	Mid-magnet-to-pole ratio, $[-]$
A_z	Axial magnetic vector potential, $[\mathrm{Wb/m}]$
B_r	Remanent flux density of magnets, [T]
c_{mn}, d_{mn}	Unknown harmonics coefficients $[\mathrm{Wb/m}]$
C_m	Boundary condition field coefficient, $[\mathrm{Wb/m^2}]$
f, f_{sw}	Fundamental and switching frequency, [Hz]
H	Harmonic order referred to the rotor $[-]$
i, h	phase current & current harmonic [A]
j	imaginary unit $[-]$
J_0, J_a, J_e	Induced, reaction field, & total eddy currents density $[\mathrm{A/mm^2}]$ or [A]
k_e	Emf constant for peak fundamental, $[\mathrm{Nm/A}]$
k_t	Torque constant using rms current, $[\mathrm{Nm/A}]$
l_a	Active machine length, $[\mathrm{mm}]$
L_s	Per phase armature inductance, [H] or [pu]
m, M	Space harmonic & total number $[-]$
n, N	Time harmonic & total number $[-]$
p, N_s	Number of pole pairs and series turns, $[-]$
P_e	Mean eddy currents loss [W]
r	Radial coordinate position, $[\mathrm{mm}]$ or $[\mathrm{m}]$
R_i, R_r, R_m	Inner radius, inner magnet, & outer magnet radius, $[\mathrm{mm}]$
R_s, R_w	Inner winding & outer winding radius, $[\mathrm{mm}]$
R_y, R_o	Yoke & outer stator radius, $[\mathrm{mm}]$
t, T, T_{sw}	Instantaneous time instant, electrical time period, & switching time period [s]
U_d, U_q, U_{svm}	D-axis voltage, Q-axis voltage, & SVM voltage (rms), [V] or [pu]
V_{dc}	Inverter's DC link voltage, [V] or [pu]
$x = 1, 2, 3$	motor phase index $[-]$

M. Leandro and J. K. Nøland are with the Department of Electric Power Engineering, Norwegian University of Science and Technology (NTNU), Trondheim, Norway (e-mail: matteo.leandro@ntnu.no; jonas.k.noland@ntnu.no).

I. INTRODUCTION

CONTROL of electrical machines through power inverters comes along with several challenges stretching from system design to application adaptation. On the design side, machine designers are asked to incorporate an understanding of the final motor operation to know the inverter's impact on the overall performance. In some cases, the whole motor-inverter system ought to be designed as a whole to find the best trade-off on both subsystems. The assessment of motor performance under inverter operation represents a task that can be handled effectively by means of circuit-coupled finite element analysis (FEA) [1]. However, due to its time intensiveness, it cannot be the first step in rapid design processes. When obtaining a quick initial design, one has to sacrifice accuracy to leave room for computational efficiency.

An overview of applicable methods to predict rotor eddy-current losses is presented in [2]. Analytical models represent an attractive choice as they can, under the same assumptions, meet the same accuracy as FEA with remarkable computational efficiency [3]. Under the hypothesis of linearity, two-dimensional (2-D) magnetostatic problems can be solved analytically [3]–[6]. Fourier-based analytical models solving Maxwell's equations also allow us to simulate the equivalent of a circuit-coupled time-stepping simulation [1]. When calculating induced eddy-currents in the magnets, magnet segmentation can be accounted for without including the eddy currents reaction field as in [7]–[10]. On the contrary,

solving the diffusion equation in polar coordinates allows the inclusion of eddy currents reaction field, albeit neglecting magnet segmentation [11]–[13]. Including both eddy-current reaction field and magnet segmentation is possible at the price of higher implementation, and computational complexity [14].

Several authors have also worked on developing analytical models in Cartesian coordinates to account for both magnet segmentation and eddy currents reaction field [15], [16]. However, any curvature effect is neglected. Their work highlighted that magnet segmentation might give a rather counter-intuitive loss increase. This behavior occurs in relation to high-frequency harmonics introduced by power converters and is considered a segmentation anomaly [17]. In fact, the loss reduction from magnets segmentation is achieved only if axial or circumferential dimensions or both are smaller than twice the skin depth [2].

Nowadays, analytical modeling of PM eddy currents loss is considered a well-developed topic. Nevertheless, it appears unusual for authors to contextualize these models to a realistic inverter-fed operation, a significant limitation in the literature. To the authors' knowledge, only one brief example does not overlook the need to incorporate realistic analytical inverter outputs to feed the eddy currents problem [18]. However, the inverter output was not simplified in this approach.

In this paper, a generalized three-phase inverter model with space vector modulation (SVM) is developed. The inverter model can be considered semi-analytical, and the output is conveniently post-processed to fit the proposed eddy currents formulations in the most general way. The symmetrical components analysis is performed on the harmonic spectrum of the three-phase current waveform. The presented methodology defines a complete framework where the inverter model uses parameters from the motor obtained from analytical magnetostatic models. Those include the back-emf constant and machine inductances. The parameters define real current waveforms resulting from steady-state operating conditions.

The case study presented in this paper centers on slotless PM machines equipped with a Halbach array rotor. These machines offer various desirable qualities, including the elimination of cogging and magnets losses due to slotting effects, which can typically restrict a motor's operating speed [19]. However, the inverter-fed operation of these machines produces a high current ripple that emphasizes the importance of the PM eddy current analysis presented in this study.

The paper's main contribution is to provide insights into the numerical challenges of implementing analytical eddy-current models in polar coordinates, as they are overlooked in the literature. Two popular modeling strategies are shown focusing on resolving numerical inaccuracies arising from an extended model like the one presented in the following. The inverter-fed operation, with an accurate inverter model, contextualize the analysis to a realistic case study, thus giving further support to the importance of the proposed research. Finally, we propose a way to make the inverter output suitable to be an input to the popular eddy-current models with the possibility of simulating any steady-state operating condition. Transient modeling of PM eddy-current losses is outside the scope of this paper. The application of slotless machines makes saturation less of a concern, given the weak armature reaction field. The two-dimensional modeling should be coupled to suitable correction factors or models to account for three-dimensional axial leakage.

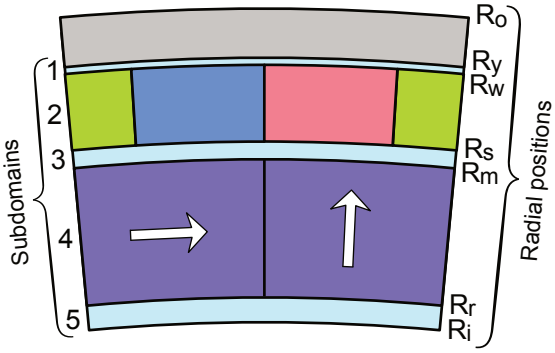

Fig. 1. Subdomain/layers subdivision of the studied slotless inrunner PM machine for analytical field formulation with radial positions indicated.

The paper is structured as follows. Section II provides an introduction to analytical eddy-current models, highlighting the unique contributions of this study in comparison to existing literature. This section also outlines the need for the proposed inverter model. Section III presents the inverter model and our approach to generalizing its output. Section IV serves as a short introductory guide to the published codes. Finally, Section IV presents the results of the developed analytical eddy-current models, followed by the concluding remarks in Section V.

II. State-Of-The-Art Eddy Current Models In Polar Coordinates and Paper's Contribution

Analytical eddy currents modeling through Fourier-based formulations have long been attractive [2]. The different governing equations applied in regions where the eddy currents are estimated allow us to neglect or account for the eddy-current reaction field. This paper assumes that the region of the magnet is the only one affected by the eddy currents. However, conductive magnets sleeve and magnets support should be considered if part of the assembly. Consequently, the eddy currents occur in the region of the magnets, i.e., region 4 in Fig. 1. Assuming the problem's source is only the stator current field, eq. (1) is the governing equation in the region of the magnets.

$$\nabla^2 A_z = -\mu_0 \mu_r \sigma \frac{\partial A_z}{\partial t} \tag{1}$$

Eq. (1) reduces to the Laplace equation ($\nabla^2 A_z = 0$) by assuming zero magnets conductivity. It means that no induced eddy currents are included.

This paper's two main contributions are as follows.

1) For the model neglecting the eddy-current reaction field, the Gibbs phenomenon introduces uncertainty. A solution to the problem is presented, along with a results comparison highlighting the improvement.
2) For the model accounting for the eddy-current reaction field, the dependency of the field formulation on Bessel's functions makes it necessary to resort to specific software toolboxes to achieve the best accuracy. The catas-

TABLE I
SPM MACHINE DATA (COURTESY OF ALVA INDUSTRIES)

$\mathbf{R_r}$	$\mathbf{R_m}$	$\mathbf{R_s}$	$\mathbf{R_w}$	$\mathbf{R_y}$	$\mathbf{R_o}$	$\mathbf{l_a}$	$\mathbf{p}$	$\mathbf{B_r}$	$\boldsymbol{\mu_r}$	$\boldsymbol{\xi_{pm}}$	$\boldsymbol{\sigma_{pm}}$	$\mathbf{N_s}$
39.0 mm	41.8 mm	42.2 mm	43.79 mm	43.83 mm	44.8 mm	15.2 mm	17	1.35 T	1	0.5	0.667 MS/m	3

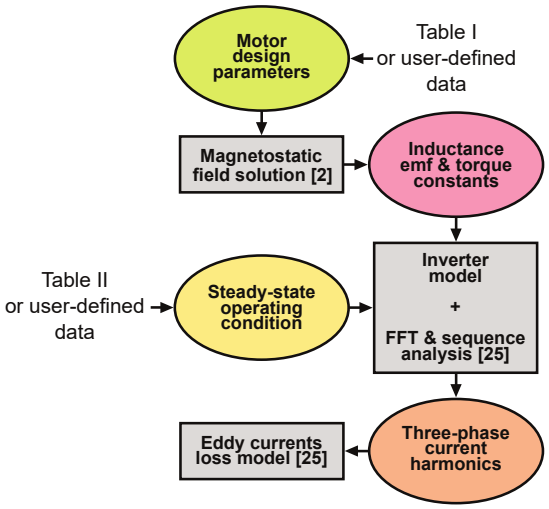

Fig. 2. Flowchart of the workflow of the whole semi-analytical framework made available at [26].

trophic numerical error produced in double-precision arithmetic is emphasized with a proposed solution to fix the problem.

For both cases in eq. (1), the three-phase current density, acting in the winding region (region 2), is assumed to be the only source of the problem. The resulting current density expression can be expressed as in [3], [20], yielding

$$J(\vartheta, t) = \sum_{n,m} J_{n,m} \cos[n\omega t + \varphi_n + k\alpha]. \tag{2}$$

In earlier works, the only realistic inverter voltage considered was the naturally sampled pulse-width modulation (PWM) [18], [21]. The same double Fourier analytical inverter output can also be developed for SVM inverter control [22]. As different inverter outputs result from different SVM vectors placement [23], it appears to be easier to resort to a semi-analytical inverter modeling [24], [25]. The next section focuses on the post-processing of the SVM inverter output into a suitable form for the eddy-current models.

All the useful machine data are reported in Table I, and the derived values of back-emf constant, torque constant, and phase inductance are reported in Table II, along with the simulated operating point. Fig. 2 shows schematically the whole inverter model framework for the eddy currents loss estimation we present herein. It is meant to be the first tile of a complete model where all the motor losses are estimated and synergically coupled to a thermal model for parameter correction with the temperature at any operating condition.

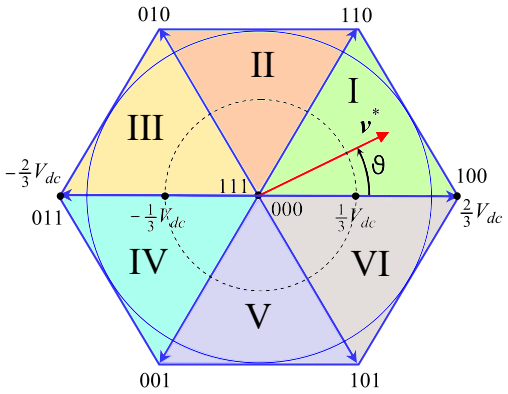

Fig. 3. Space vector diagram of the considered three-phase power inverter.

III. INVERTER MODELING FOR SVM CONTROL

As mentioned before, the Fourier-based analytical model describing the magnet's eddy-current losses requires the field source to be described as a harmonic series; there are two ways to model the three-phase inverter output. In both instances, the inverter switches are assumed to be ideal devices switching from on to off state instantly without considering the existence of a dead time to avoid a short circuit of the DC-link; this assumption is valid if dead-time compensation is implemented in the chosen inverter. A fully analytical approach exists and is based on a double Fourier integral analysis [21], [27], [28].

Unlike this purely analytical approach, the model described and employed in this work is a semi-analytical model inspired by existing SVM modeling practices [23]–[25]. We analytically define each switching state's timing to replicate the sinusoidal steady state reference voltage. The resulting output voltage is made of a stream of pulses resulting from the inverter commutation. The estimated current resulting from this voltage applied to the motor terminals is then analyzed through FFT analysis. The following section describes the procedure to develop the proposed SVM model, with a closer look at the numerical implementation in the published script (Inverter_star_VESC.m) [26].

A. Inverter Output Implementation

As mentioned, SVM offers remarkable flexibility in its implementation as one can choose where to place the different inverter states in time within each switching interval. The switching can be optimized for harmonic content or switching losses. The inverter model is benchmarked against an off-the-shelf motor controller, i.e., *Vedder Electronic Speed Controller – VESC 6 Mk V*, that implements an inverter control strategy aimed at minimizing the switching events when transitioning between the different states and implements a dead-time compensation [29]. The commutation scheme

TABLE II
DERIVED VALUES FOR THE MACHINE, THE INVERTER AND THE EXAMINED OPERATING POINT IN THIS CASE STUDY

$\mathbf{k_t}$	$\mathbf{k_e}$	$\mathbf{V_{dc}}$	$\mathbf{\Re_s}$	$\mathbf{L_s}$	$\boldsymbol{\tau_m}$	$\mathbf{n_s}$	$\mathbf{f}$	$\mathbf{f_{sw}}$
0.0724 Nm/A	0.0483 Vs	45 V	10 mΩ	4.6 μH	3 Nm	2500 rpm	833.33 Hz	10 kHz

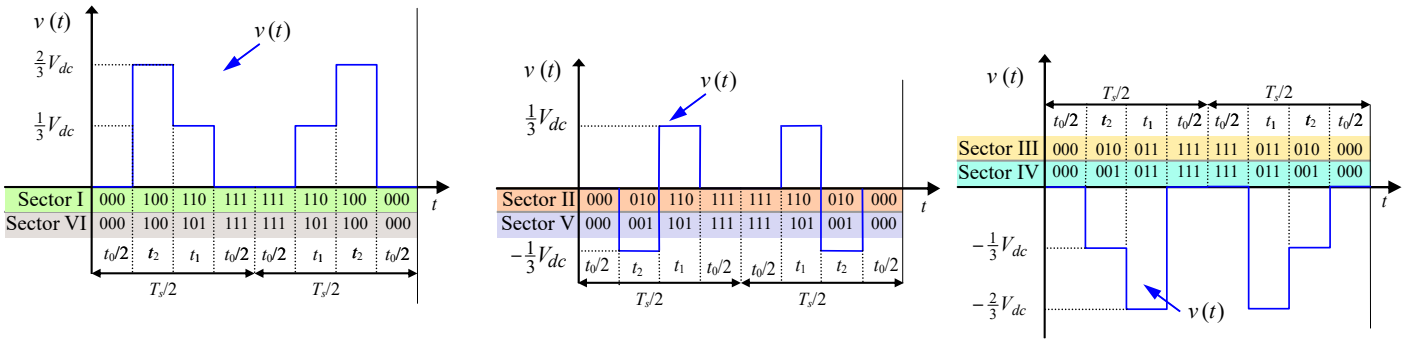

Fig. 4. Sequence of active and zero states within each switching period for the different sectors in Fig. 3 with their respective voltages on phase a. It highlights the commutations within different sectors (i.e., Sectors I & VI, Sectors II & V, and Sectors III & IV) lead to the same phase-voltage waveform.

between different states shown in Fig. 3 is presented in Fig. 4 referring to a single phase. The same switching sequence described in [24] is implemented in this algorithm. Therefore, the equations for the different timings (t_0, t_1, t_2) shown in [24] can be equally used. The numerical implementation becomes straightforward as a whole fundamental period can be divided into switching periods whereon the reference voltage is sampled and the different timings are evaluated. The different states to apply over each instant depend on the location of the reference voltage in the vector plane according to Fig. 3. The reference voltage is estimated considering a maximum torque per ampere (MTPA) control of a surface-mounted permanent magnet motor (SPM) where the current is all directed in the quadrature axis ($I = I_q$). The steady state voltage equation in the dq reference frame are

$$U_d = -2\pi f L_s I, \quad U_q = \Re_s I + \frac{2\pi f}{p} k_e, \\ \tau_m = k_t I, \quad U_{svm} = \sqrt{U_d^2 + U_q^2} \tag{3}$$

All parameters are estimated analytically by means of the field solution presented in [3] through the methodology described in [30], [31]. These steps, along with the whole workflow of the proposed framework, are presented in Fig. 2. The inverter model gives a stream of pulses as an output, and the resulting current ripple is estimated by integrating the instantaneous voltage of each phase divided by the phase inductance [24].

The inverter model is tested with a motor with the parameters listed in Table II. The results in Fig. 5 compares the measured waveform with the one simulated. The comparison is extended to the total RMS value of the current waveform and THD percentage in Table III to remark on the good accuracy of the proposed model

The output of the inverter model needs to be post-processed through the FFT to get the Fourier coefficients of the current waveforms. One could notice that a perfectly periodic current waveform is only obtained if the fundamental period is a multiple of the switching period, which is hardly ever the case. If the model produced a non-periodic current waveform, the loss analysis would generate non-negligible inaccuracies due to the Fourier series trying to force the signal to be periodic. Nevertheless, the inverter model we propose [26] implements a clever way of framing the current waveform within the fundamental period to make sure that the resulting waveform is symmetric. In this way, the methodology achieves the maximum accuracy. It can be proved that the harmonic analysis of the current waveform through FFT has to be performed for at least two phases, as they are not a mere phase shift of 120° of one phase waveform. As a result, the three-phase current waveform can be expressed as:

TABLE III
COMPARISON OF INVERTER MODEL AT 30 kHz SWITCHING FREQUENCY AGAINST MEASURED WAVEFORM IN FIG. 5

Data	RMS	THD
Measured waveform	20.80 A	27.40 %
Inverter model	20.84 A	27.10 %
Deviation	+0.19 %	-1.09 %

$$i_x(t) = \sum_n \{h_{x,n} \cos[n\omega t + \varphi_{n,x}]\} \tag{4}$$

In this scenario, the three-phase current density distribution from the stator winding, including both time harmonics and space harmonics, can be defined as follows [3]:

$$J_x(t,\vartheta) = \sum_{n,k} \{J_{x,n,k} \cos[n\omega t + \varphi_{n,x}] \cdot \\ \cdot \cos[k(p\vartheta - (x-1)2/3\pi)]\} \tag{5}$$

From the latter expression, it is impossible to obtain a resulting current density distribution that gathers the contribution of the three phases in one term; therefore, the field solution needs to be studied as the sum of the contribution from the three phases separately. This makes the post-processing of the field

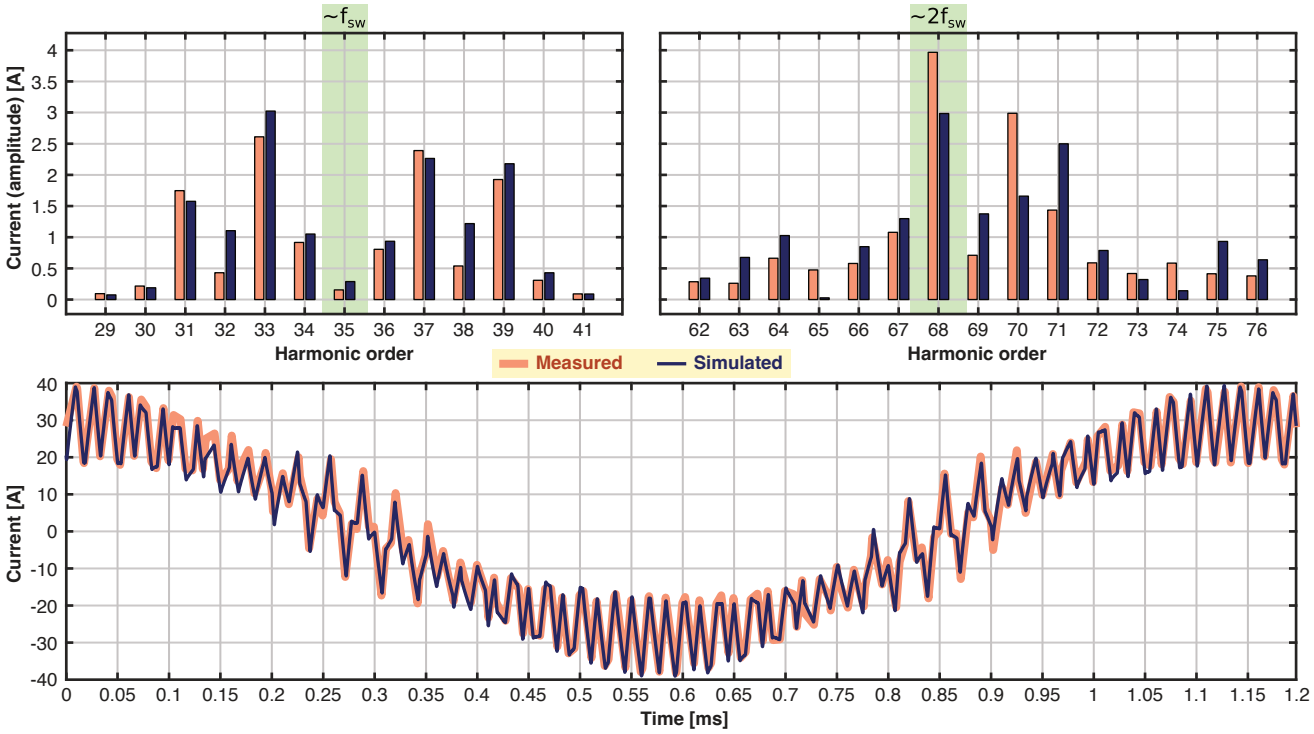

Fig. 5. Measured phase current waveform (courtesy of Alva Industries) compared against the simulated waveform in the time domain and in the frequency domain, highlighting the main harmonics around f_{sw} and $2f_{sw}$, with 30 kHz switching frequency, 3100 rpm motor speed, and 2.21 Nm reference torque.

solution more tedious and the analytical models presented in the literature useless.

B. Inverter Output Analysis By Symmetrical Components

One could observe that the output of the inverter model provided in [26] is not the same as one would get by taking a single-phase waveform and shifting it by ± 120 degrees for the other two phases. This suggests that the system can be analyzed through its symmetrical components, i.e., positive, negative, and zero sequence components. Starting from the three-phase currents (4) written in phasor form:

$$\bar{I}_x = \sum_n h_{x,n} e^{j[\omega t + \varphi_{n,x}]} \tag{6}$$

It is possible to describe the three-phase system as the contribution of positive (or direct), negative (or inverse), and zero-sequence (or homopolar) components as follows:

$$\begin{aligned} \bar{I}_0 &= \frac{\bar{I}_1 + \bar{I}_2 + \bar{I}_3}{3} = 0 \\ \bar{I}_d &= \frac{\bar{I}_1 + \beta \bar{I}_2 + \beta^2 \bar{I}_3}{3} = \sum_n I_{d,n} e^{j[\omega t + \varphi_{n,d}]} \\ \bar{I}_n &= \frac{\bar{I}_1 + \beta^2 \bar{I}_2 + \beta \bar{I}_3}{3} = \sum_n I_{i,n} e^{j[\omega t + \varphi_{n,i}]} \end{aligned} \tag{7}$$

where $\beta = e^{j2pi/3}$. The zero-sequence component is always zero assuming the ideal case of a star-connected motor with an isolated neutral point. In this way, one can re-write the three-phase currents in (6) as:

$$\begin{aligned} \bar{I}_a &= \bar{I}_0 + \bar{I}_d + \bar{I}_i \\ \bar{I}_b &= \bar{I}_0 + \beta^2 \bar{I}_d + \beta \bar{I}_i \\ \bar{I}_a &= \bar{I}_0 + \beta \bar{I}_d + \beta^2 \bar{I}_i \end{aligned} \tag{8}$$

Having the three-phase currents expressed as a combination of direct and inverse components allows rewriting the three-phase current density distribution (2) as $J(\vartheta, t) = J_d(\vartheta, t) + J_i(\vartheta, t)$; where $J_d(\vartheta, t)$ and $J_i(\vartheta, t)$ can be expressed in the time domain as:

$$\begin{aligned} J_d(\vartheta, t) = \sum_x \{ & J_d \cos[n\omega t + \varphi_{nd} - (x-1)2\pi/3] \cdot \\ & \cdot \cos[k(\omega t + \alpha - (x-1)2\pi/3)] \} \\ J_i(\vartheta, t) = \sum_x \{ & J_i \cos[n\omega t + \varphi_{ni} + (x-1)2\pi/3] \cdot \\ & \cdot \cos[k(\omega t + \alpha - (x-1)2\pi/3)] \end{aligned} \tag{9}$$

The latter expressions make it easy to highlight the combination of time and space harmonics which contribute to the magneto-motive force. In particular, taking the direct-sequence component as an example, by means of some trigonometric identities, $J_d(\vartheta, t)$ can be rewritten as the sum of a forward rotating component $J_{fd}(\vartheta, t)$ and a backward rotating component $J_{bd}(\vartheta, t)$:

$$\begin{aligned} J_{(f,b)d}(\vartheta, t) = \frac{J_d}{2} \{ & \cos[k\alpha \mp n\omega t \mp \varphi_{nd}] \\ & + \cos[k\alpha \mp n\omega t \mp \varphi_{nd} - (k \mp 1)2\pi/3] \\ & + \cos[k\alpha \mp n\omega t \mp \varphi_{nd} + (k \mp 1)2\pi/3] \end{aligned} \tag{10}$$

which takes the minus sign for the forward-rotating component and the plus sign for the backward-rotating one.

The harmonics giving a non-zero contribution and the related current density expressions are reported in the following for the direct-sequence and inverse-sequence component:

$$\left.\begin{aligned} J_{fd} &= \tfrac{3J_d}{2}\cos\left[k\alpha - n\omega t - \varphi_{nd}\right], k-1=3L \\ J_{bd} &= \tfrac{3J_d}{2}\cos\left[k\alpha + n\omega t + \varphi_{nd}\right], k+1=3L \end{aligned}\right\} L\in\mathbb{Z} \tag{11}$$

$$\left.\begin{aligned} J_{fi} &= \tfrac{3J_i}{2}\cos\left[k\alpha - n\omega t - \varphi_{ni}\right], k+1=3L \\ J_{bi} &= \tfrac{3J_i}{2}\cos\left[k\alpha + n\omega t + \varphi_{ni}\right], k-1=3L \end{aligned}\right\} L\in\mathbb{Z} \tag{12}$$

Finally, the three-phase current density distribution can be conveniently expressed in the rotor reference frame ϑ considering that $\alpha = \omega t + p\vartheta$ as follows:

$$J_z(\vartheta, t) = \boldsymbol{J}_{nm}\cos\left[\boldsymbol{H}\omega t + \boldsymbol{\varphi} + \boldsymbol{k}p\vartheta\right] \tag{13}$$

where $\boldsymbol{J}_{nm}$, $\boldsymbol{H}$, $\boldsymbol{\varphi}$ and $\boldsymbol{k}$ are all matrices holding the respective values satisfying (11) and (12) for each time and space harmonic order, meaning that they will have size $4\times M\times N$. In particular, all the models were shown to deliver accurate solutions with $M=3$, while N is found as follows to achieve a good resolution of the current spectrum:

$$N \approx 100\cdot\frac{T}{T_{sw}} \tag{14}$$

The following analysis is based on the number of harmonics chosen as in eq.(14). The value brings the loss analysis close to the convergence; however, a slight variation can be expected when increasing the number of harmonics. It is advised against reducing the number of harmonics to avoid filtering the current data in the models.

IV. Analytical Eddy Currents Model

In this section, the two main modeling techniques for analytical eddy currents loss estimate are thoroughly described, focusing on their limitations and proposed improvements.

A. Analytical Model Excluding Eddy Currents Reaction Field

First, we will focus on an approach where the eddy currents losses are not evaluated as a mere contribution of each and every harmonic of the field. Still, they also account for the interaction between the combination of time and space harmonics having the same frequency in the rotor reference frame [7]. This way of modeling is needed to achieve the best accuracy. In addition, the inverter output from SVM control makes it necessary to adapt the model for numerical implementation as a non-negligible deviation was found in comparison against FEA [7]. According to [3], solving the problems presented in Appendix A leads to the following expression for the one-component magnetic vector potential

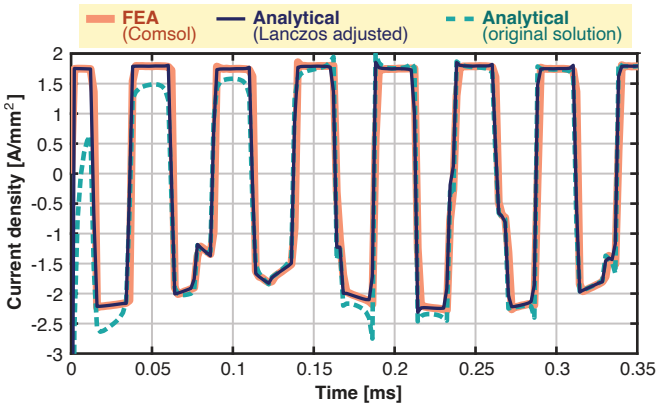

Fig. 6. Comparison of induced current density (J_0) in the middle of the mid-magnet over a quarter of the electrical period. FEA is compared against the analytical solution and the adjusted solution through the Lanczos factor.

in the region of the magnets:

$$A_z = \frac{R_w}{m}\left[\left(\frac{r}{R_w}\right)^m + \left(\frac{R_i}{R_w}\right)^m\left(\frac{R_i}{r}\right)^m\right]C_m \cos\left(H\omega t + \varphi + m\vartheta\right) \tag{15}$$

Induced eddy currents in the magnets are formulated in eq. (16) [7]. The explicit expressions of J_0 and J_a are reported in Appendix B.

$$J_e = J_0 + J_a = -\sigma\frac{\partial A_z}{\partial t} + \kappa(t) \tag{16}$$

The net zero coefficient in eq. (17) assumes that the different segments are insulated from one another.

$$\kappa(t) = \frac{2}{\alpha_m(R_m^2 - R_r^2)}\int_{\vartheta_1}^{\vartheta_2}\int_{R_r}^{R_m}\sigma\frac{\partial A_z}{\partial t}r\,dr\,d\vartheta \tag{17}$$

To avoid the non-negligible Gibbs phenomenon in the time derivative of A_z, the expressions must be improved for numerical implementation by multiplying them by the Lanczos factor (λ). An effective Lanczos factor is expressed in eq. (18).

$$\lambda = \left[\frac{\sin\left(\pi n/N\right)}{\pi n/N}\right] \tag{18}$$

The effectiveness of introducing λ is highlighted in Fig. 6, where the induced current density J_0 is plotted over the middle point of the mid-magnet over a quarter of the electric period.

In addition to Fig. 6, Fig. 7 and Table IV map the induced current density and the deviations for a given time instant. The improved analytical model is significantly closer to the FEA model than the standard one. It can be noticed that the improved model shows a relatively high relative deviation of the induced eddy current density where this approaches zero, meaning that in absolute value is negligible.

The eddy currents mapped over the magnet region result in an average induced magnet loss (for each segment spanning from ϑ_1 to ϑ_2) that can be computed according to eq. (19) [7].

$$P_e = \frac{l_a\omega_r}{2\pi\sigma}\int_0^{2\pi/\omega_r}\int_{\vartheta_1}^{\vartheta_2}\int_{R_r}^{R_m}J_e^2 r\cdot dr\cdot d\vartheta\cdot dt \tag{19}$$

Eq. (19) is now utilized with the improved eddy currents model proposed in this paper. Table V reveals the differ-

TABLE IV
MEAN ABSOLUTE EDDY CURRENT DEVIATION OF ANALYTICAL MODELS EXCLUDING THE REACTION FIELD AGAINST FEA (J_z MAP IN FIG. 7)

Model	Mid-magnet	Side-magnet
Improved model	7.0 %	3.2 %
Standard model [7]	35.5 %	22.6 %

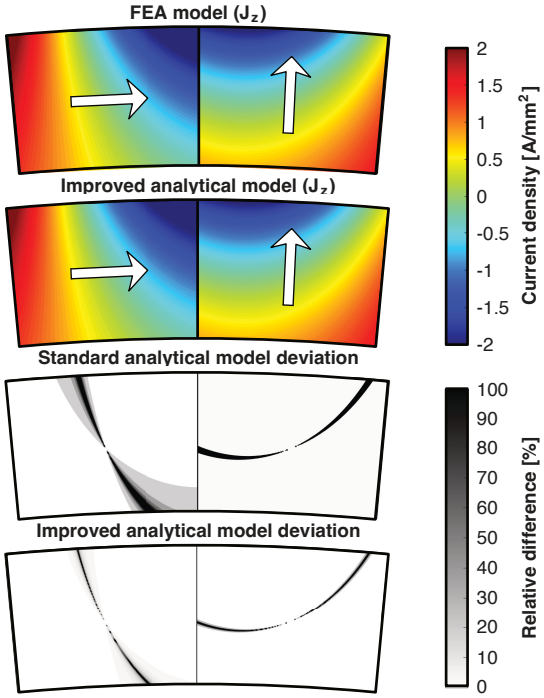

Fig. 7. Induced current density (J_z) map in the region of the magnet excluding the eddy currents reaction field for time instant, $t = 182.23\,\mu$s, after initiation of simulation. The upper maps show comparison between the FEA model and the improved analytical model. The lower maps highlight the relative difference with the FEA model as a reference, comparing the standard model against the improved model.

ence in the eddy currents loss estimate when the improved analytical model is implemented. Despite the diligent care taken to ensuring the best accuracy of the analytical model, we deemed it necessary to consider FEA as the reference model because of the imperfect periodicity given by the output of the inverter model, which causes a small error in the loss analysis. Moreover, the errors in the eddy current density map do not propagate with the same magnitude on the loss analysis. A high relative error is mostly bounded around small current density values for any instant. For total transparency and replication, the code implementation of the standard and improved model are available as "No_react.m" and "IMPROVED_no_react.m", respectively [26].

B. Analytical Model Solving the Diffusion Equation

The problem expressed in eq. (1), when the right-hand-side term is different from zero, allows accounting for the eddy currents reaction field under the fundamental assumption of having a homogeneous magnetic ring. To simplify the resolution of the differential equation, the source current density in

TABLE V
EDDY CURRENTS LOSS ESTIMATE (EXCL. REACTION FIELD) AT 10 kHz SWITCHING FREQUENCY AGAINST REFERENCE MODEL AND FEA

Model	Loss Value	Deviation
FEA model	11.92 W	0.0 %
Standard model [7]	12.48 W	+5.0 %
Improved model	11.87 W	-0.4 %

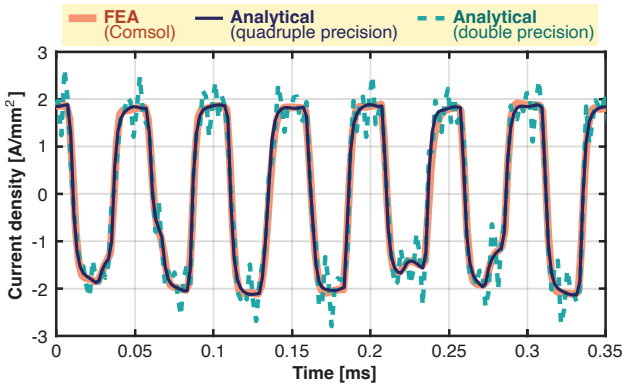

Fig. 8. Comparison of induced current density (J_z) in the middle of the mid-magnet over a quarter of the electrical period. FEA is compared against the analytical solution obtained in double precision and in quadruple precision with Advanpix.

eq. (13) is expressed in the complex form in eq. (20).

$$J_z(\vartheta, t) = \mathbb{R}\{\boldsymbol{J}_{nm} e^{j[\boldsymbol{H}\omega t + \boldsymbol{\varphi} + \boldsymbol{k}p\vartheta]}\} \tag{20}$$

As the solution to eq. (1) holds the same form as the source of the field, namely the stator current density in eq. (20), the equation is conveniently rewritten in eq. (21) as the Bessel equation form.

$$r^2 \frac{\partial^2 A_z}{\partial r^2} + r \frac{\partial A_z}{\partial r} + (r^2\delta^2 - m^2) A_z = 0 \tag{21}$$

The inverse to the skin depth is defined in eq. (22) [32].

$$\delta = j^{3/2} \sqrt{H \omega \mu_0 \mu_r \sigma} \tag{22}$$

As thoroughly shown in several other works [32]–[35], the solution to eq. (21) is expressed in eq. (23).

$$A_z(\vartheta, r, t) = [c_{mn} \mathbb{J}_m(\delta r) + d_{mn} \mathbb{Y}_m(\delta r)] e^{j[\boldsymbol{H}\omega t + \boldsymbol{\varphi} + \boldsymbol{k}p\vartheta]} \tag{23}$$

It is worth noting that when $H = 0$, i.e., for all the combinations of time and space harmonics rotating synchronously with the rotor, the governing differential equation is the Laplace equation, and the magnetic potential in the region of the magnets can be expressed as in eq. (24).

$$A_z(\vartheta, r, t) = \left[c_{mn} \left(\frac{r}{R_m} \right)^m + d_{mn} \left(\frac{R_r}{r} \right)^m \right] e^{j[\boldsymbol{\varphi} + \boldsymbol{k}p\vartheta_r]} \tag{24}$$

The equations resulting from the boundary conditions are reported in Appendix A, eq. (32). The system can be either solved numerically for each and every existing combination of time and space harmonics or symbolically, thus leading to analytical expressions holding for every harmonic coefficient. The latter method is the most computationally efficient as the system is solved once and for all. The coefficients in the

TABLE VI
EDDY CURRENTS LOSS ESTIMATE (EXCL. MAGNETS SEGMENTATION) AT 10 kHz SWITCHING FREQUENCY AGAINST REFERENCE MODEL AND FEA

Model	Loss Value	Deviation
FEA model	38.56 W	0 %
Double precision model (28)	41.53 W	+7.7 %
Quadruple precision model (28)	38.44 W	-0.3 %

TABLE VII
MEAN ABSOLUTE EDDY CURRENT DEVIATION OF ANALYTICAL MODELS INCLUDING THE REACTION FIELD AGAINST FEA (J_z MAP IN FIG. 9)

Model	Deviation
Improved model (quadruple precision))	3.4 %
Standard model (double precision) [7]	198.0 %

regions of interest can be used without solving the whole field problem every time. Regardless of the way to solve the system of equations, having Bessel functions in the field formulations adds a numerical issue that has not yet been addressed in the literature when presenting analytical models solving the diffusion equation. As shown in [36], double precision arithmetic fails at evaluating Bessel functions accurately. The presented eddy currents model uses the Multiprecision Computing Toolbox (Advanpix) to evaluate Bessel functions accurately and reliably estimate the eddy currents loss in quadruple precision arithmetic.

According to Poynting's theorem in eq.(25), the rotor eddy current loss can be effectively estimated. (25) [34].

$$P_e = \frac{1}{2\sigma} R_m l_a \mathbb{R}\left\{\int_0^{2\pi} (J_z H_\vartheta^*)_{r=R_m} d\vartheta\right\} \tag{25}$$

$$H_\vartheta = -\frac{1}{\mu}\frac{\partial A_z}{\partial r} \tag{26}$$

$$J_z = -\sigma \frac{\partial A_z}{\partial t} \tag{27}$$

From eq. (26) and (27), (25) can be rewritten into eq. (28).

$$P_e = \frac{p\omega_r \pi R_m l_a \boldsymbol{H}}{\mu} \mathbb{R}\{[c_{mn}\mathbb{J}_m(\delta R_m) + d_{mn}\mathbb{Y}_m(\delta R_m)] [c_{mn}\mathbb{J}'_m(\delta R_m) + d_{mn}\mathbb{Y}'_m(\delta R_m)]^*\} \tag{28}$$

Under the same operating point detailed in Table II, the FEA model of the motor with specifications listed in Table I was set assuming a conductive homogeneous magnet ring, thus neglecting the segmentation but considering the eddy currents reaction field. The analytical model is benchmarked against FEA, similar to the previous section.

In Fig. 8, the current density in the middle of the mid-segment is plotted over a quarter of an electrical period. It can be noted how the eddy current density computed in double precision arithmetic exhibits a remarkable deviation, while the same expression computed in quadruple precision (Advanpix) is in good correspondence with the results obtained in FEA.

The total induced magnets loss was computed through eq. (28). Table VI compares the result obtained through FEA taken as a reference to show the deviation of the multi-precision model and the same model computed in double precision.

As proposed for the previous model, to enrich the analysis, the comparison between the induced current density maps is presented in Table VII and Fig. 9. The current maps are plotted for the same instant taken for the previous model to show the different current distributions estimated with this model. It is hard to notice any difference between the current map obtained through FEA and the improved model. The mean deviation of the standard model is shown in Table VII to be 58 times larger than the improved model.

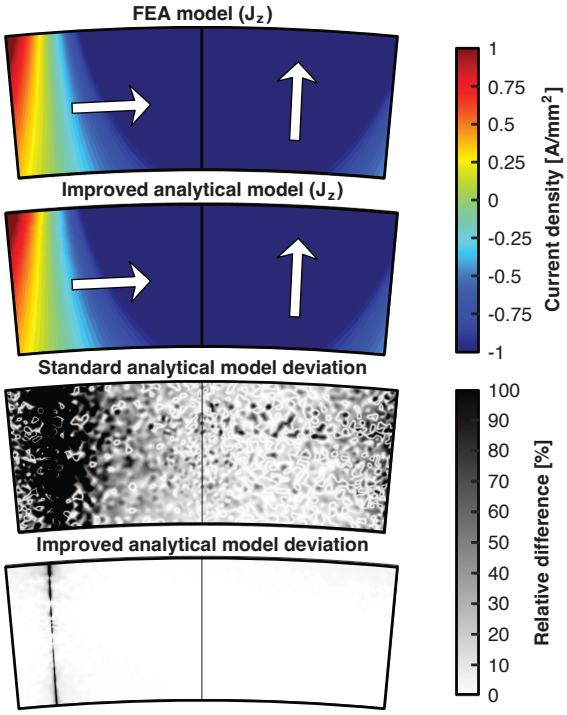

Fig. 9. Induced current density (J_z) map in the region of the magnet including eddy currents reaction field for time instant, $t = 182.23\,\mu$s, after initiation of simulation. The upper maps show a comparison between the FEA and the improved analytical models. The lower maps highlight the relative difference with the FEA model as a reference, comparing the standard model (double precision) against the improved model (quadruple precision).

The error map remarks on the need to use multi-precision arithmetic tools to accurately compute Bessel functions and any mathematical expression dependent on them. The analytical model accounting for the eddy currents reaction field is not appropriate for the specific case study, which considers a segmented Halabch array, as the segmentation impact on the final loss estimate is neglected. Nevertheless, the case study was taken to fully address numerical issues arising from developing two popular analytical eddy currents models. The analytical model implemented in double precision is published as Double_precision_with_reaction.m [26]. The multi-precision version of it could not be published as Advanpix is not available in Code Ocean. However, its implementation requires the minimal change of specifying the argument of the Bessel's functions in the code as multi-precision arguments.

C. Eddy-Currents Reaction Field and Segmentation

As pointed out in the introduction, it is possible to include the circumferential magnets segmentation typical of a Halbach array and the induced eddy currents reaction field in one model. The drawback is a greater computational complexity which might lead to a non-negligible runtime slowdown if coupled with a multiple-precision arithmetic implementation. Nevertheless, the basis for developing such a model is presented in [14]], and any Bessel's function should be computed with suitable tools to avoid inaccuracies from their computation. The analysis was performed through FEA to give an idea of what to expect from a model accounting for eddy-currents reaction field and segmentation for this specific case study. The loss analysis gave a total loss value of $12.3\,\mathrm{W}$, which is very close to the value shown in Table IV. The result is unsurprising, considering the reasoning presented in cite7947717. In fact, the motor presented in our study has an angular magnet thickness of about $4\,\mathrm{mm}$, while the skin depth is calculated from eq. (22) at the switching frequency of $10\,\mathrm{kHz}$ is about $4.4\,\mathrm{mm}$. Since the magnet thickness is smaller than twice the skin depth, segmentation is not considered effective for eddy-current loss reduction. The model neglects the eddy-currents reaction field results to be suitable for this particular case.

V. Published Codes

The executable version of the eddy-current models presented in this paper is available as a published capsule in Code Ocean [26]. The output of a reproducible run consists of most of the results presented in the paper, apart from the multiple-precision-based eddy currents model, due to the need for the Advanpix toolbox. The model is coded in MATLAB and it is possible for the user to duplicate the capsule and edit the input data to test the flexibility of the models. The input data are hard-coded in predefined scripts. The motor data can be modified within the "*Inrunner.m*" script, while the operating point and the inverter switching frequency can be found and modified in the inverter script "*Inverter_star_3f.m*". These models are in continuous development and are also available in GitHub [37] where further improvements are always up to date.

VI. Conclusion

The paper investigates two popular 2-D sub-domain models in polar coordinates for estimating induced eddy current losses in slotless PM machines. Our work presents a general approach to deliver the uttermost achievable accuracy using analytical techniques. The proposed approach features a synergy between different analytical models to set the foundation for fast and accurate electric drive performance assessment.

An inverter model simulating state-of-the-art switching algorithms is coupled with magnetostatic analytical models to simulate steady-state operation. The output of the inverter model is conveniently processed as an input to the analytical eddy-currents models to study the impact of the current ripple in the magnets' eddy-current losses. One model neglects the eddy currents reaction field, while the other neglects the magnets segmentation along the circumferential direction. These assumptions make the two models inappropriate for estimating the induced eddy-current losses in segmented Halbach arrays. Nevertheless, this paper has fully addressed all the challenges that may arise from implementing these two models. The impact of the Gibbs phenomenon in the first model has been highlighted, and a practical approach for mitigating it has been presented. On the other hand, the implementation of the model accounting for the eddy-currents reaction field showed a significant flaw when implemented in double-precision arithmetic. Advanpix is proposed as a solution to compute the field formulation accurately. The same proposed solution can be applied to a sub-domain model where segmentation and eddy-current reaction field can be accounted for together.

The developed models are ready to be deployed in any scenario where they can be considered to be suitable, and they will deliver the uttermost accuracy. Most code implementations are made available to encourage further development in support of all the presented findings.

Appendix A
System of Equations to Solve the Field Problem

The following boundary conditions have to be set on the boundaries separating region i from region $i+1$ to ensure the continuity of the field in the whole domain:

$$\left(B_{r(i)} = B_{r(i+1)}\right)\Big|_{r=R_{(i,i+1)}} \tag{29}$$

$$\left(H_{\vartheta(i)} = H_{\vartheta(i+1)}\right)\Big|_{r=R_{(i,i+1)}} \tag{30}$$

While on the outermost and the innermost boundaries, the assumption of infinite iron permeability allows enforcing zero tangential field components as:

$$H_{\vartheta(i)} = 0\Big|_{r=R_i, r=R_y} \tag{31}$$

the resulting system of equations is the following:

$$\begin{cases} A_1^- \left(\left(\frac{R_w}{R_y}\right)^{2m} + 1\right) = A_2^+ + A_2^- \left(\frac{R_s}{R_w}\right)^{m+1} + mA_{mJ}R_w \\ A_1^- \left(\left(\frac{R_w}{R_y}\right)^{2m} - 1\right) = A_2^+ - A_2^- \left(\frac{R_s}{R_w}\right)^{m+1} + 2A_{mJ}R_w \\ A_2^+ \left(\frac{R_s}{R_w}\right)^{m-1} + A_2^- + mA_{mJ}R_s = A_3^+ + A_3^- \left(\frac{R_m}{R_s}\right)^{m+1} \\ A_2^+ \left(\frac{R_s}{R_w}\right)^{m-1} - A_2^- + 2A_{mJ}R_s = A_3^+ - A_3^- \left(\frac{R_m}{R_s}\right)^{m+1} \\ A_3^+ \left(\frac{R_m}{R_s}\right)^{m-1} + A_3^- = ① \\ A_3^+ \left(\frac{R_m}{R_s}\right)^{m-1} - A_3^- = ② \\ ③ = A_5^+ \left(1 + \left(\frac{R_i}{R_r}\right)^{2m}\right) \\ ④ = A_5^+ \left(1 - \left(\frac{R_i}{R_r}\right)^{2m}\right) \end{cases} \tag{32}$$

The system's missing entries depend on whether the governing equation in the region of the magnet is the Laplace equation or the diffusion equation. When the diffusion equation is considered, for all those harmonics causing eddy currents, i.e., $\boldsymbol{H} \neq 0$, the entries are expressed as follows:

$$\begin{cases} ① = \dfrac{m}{R_m}(c_{mn}\mathbb{J}_m(\delta R_m + d_{mn}\mathbb{Y}_m(\delta R_m)) \\ ② = \dfrac{1}{\mu_r}(c_{mn}\mathbb{J}'_m(\delta R_m + d_{mn}\mathbb{Y}'_m(\delta R_m)) \\ ③ = \dfrac{m}{R_r}(c_{mn}\mathbb{J}_m(\delta R_r + d_{mn}\mathbb{Y}_m(\delta R_r)) \\ ④ = \dfrac{1}{\mu_r}(c_{mn}\mathbb{J}'_m(\delta R_r + d_{mn}\mathbb{Y}'_m(\delta R_r)) \end{cases} \tag{33}$$

where the derivative of the Bessel functions of the first and second kind are defined in the same way reported in the following only for the first kind Bessel function:

$$\mathbb{J}'_m(\tau r) = \frac{\delta}{2}[\mathbb{J}_{m-1}(\delta r) - \mathbb{J}_{m+1}(\delta r)] \tag{34}$$

For the case where the Laplace equation governs the field solution in the region of the magnet, i.e., supposing the magnets conductivity to be zero or for all those field harmonics rotating synchronously with the rotor ($\boldsymbol{H} = 0$), the missing entries in (32) are to be expressed as:

$$\begin{cases} ① = c_{mn} + d_{mn}\left(\dfrac{R_r}{R_m}\right)^{m+1} \\ ② = \dfrac{1}{\mu_r}(c_{mn} - d_{mn}\left(\dfrac{R_r}{R_m}\right)^{m+1}) \\ ③ = c_{mn}\left(\dfrac{R_r}{R_m}\right)^{m-1} + d_{mn} \\ ④ = \dfrac{1}{\mu_r}(c_{mn}\left(\dfrac{R_r}{R_m}\right)^{m-1} + d_{mn}) \end{cases} \tag{35}$$

Despite the several existing contributions about eddy currents modeling in the literature, a major concern has remained hidden in the implementation of (23). The issue lies in the code implementation of Bessel functions over a wide range of orders and arguments as it is needed for these models. It was shown that any programming language fails to estimate Bessel functions to a greater or lesser extent accurately. This problem has been highlighted only in [36], where the generalized inaccuracy in evaluating Bessel functions was shown for Matlab and other open-source libraries. The same problem is highlighted in the following, with a practical case showing the extreme inaccuracy achieved by headlessly developing these models in double-precision arithmetic.

APPENDIX B
INDUCED CURRENT DENSITY EXPRESSIONS

$$\begin{aligned} J_0 =& \sigma\frac{R_s}{m}\left[\left(\frac{r}{R_s}\right)^m + \left(\frac{R_i}{R_s}\right)^m\left(\frac{R_i}{r}\right)^m\right] C_m H\omega \\ & \sin\left(H\omega t + \varphi + m\vartheta\right) \end{aligned} \tag{36}$$

$$\begin{aligned} J_a =& -\frac{4\sigma}{\alpha_m(R_m^2 - R_r^2)}\frac{R_s}{m^2} f_m C_m H\omega \sin\left(m\alpha_m/2\right) \\ & \sin\left(H\omega t + \varphi + m(\vartheta_2 - \vartheta_1)/2\right) \end{aligned} \tag{37}$$

where f_m is reported in the following:

$$\begin{aligned} f_m =& \frac{1}{m+2}\left[\left(\frac{R_m}{R_s}\right)^{m+2} - \left(\frac{R_r}{R_s}\right)^{m+2}\right] + \\ & \frac{1}{2-m}\left(\frac{R_i}{R_w}\right)^{m+2}\left[\left(\frac{R_i}{R_m}\right)^{m-2} - \left(\frac{R_i}{R_r}\right)^{m-2}\right] \end{aligned} \tag{38}$$

the particular case $m = 2$ is not explicitly treated in this work.

REFERENCES

[1] A. G. Sarigiannidis and A. G. Kladas, "Switching frequency impact on permanent magnet motors drive system for electric actuation applications," *IEEE Trans. Magn.*, vol. 51, no. 3, pp. 1–4, 2015.

[2] A. Tessarolo, "A survey of state-of-the-art methods to compute rotor eddy-current losses in synchronous permanent magnet machines," in *Proc. IEEE Workshop Electr. Mach. Des. Control Diagn. (WEMDCD)*, 2017, pp. 12–19.

[3] M. Leandro and J. K. Nøland, "An approach for optimal pre-conditioning of the analytical field solution of slotless PM machines," *IEEE Access*, vol. 9, pp. 36 748–36 765, 2021.

[4] M. Leandro, N. Elloumi, A. Tessarolo, and J. K. Nøland, "Analytical iron loss evaluation in the stator yoke of slotless surface-mounted PM machines," *IEEE Trans. Ind. Appl.*, vol. 58, no. 4, pp. 4602–4613, 2022.

[5] J. Hu, F. Liu, and Y. Li, "An improved sub-domain model of flux switching permanent magnet machines considering harmonic analysis and slot shape," *IEEE Access*, vol. 9, pp. 55 260–55 270, 2021.

[6] L. Gao, Z. Cai, Y. Liang, D. Wang, Q. Niu, and J. Li, "An improved analytical model of magnetic field in surface-mounted permanent magnet synchronous motor with magnetic pole cutting," *IEEE Access*, vol. 9, pp. 142 804–142 814, 2021.

[7] L. J. Wu, Z. Q. Zhu, D. Staton, M. Popescu, and D. Hawkins, "Analytical model for predicting magnet loss of surface-mounted permanent magnet machines accounting for slotting effect and load," *IEEE Trans. Magn.*, vol. 48, no. 1, pp. 107–117, 2012.

[8] P. Madina, J. Poza, G. Ugalde, and G. Almandoz, "Magnet eddy current loss calculation method for segmentation analysis on permanent magnet machines," in *Proc. Eur. Conf. Power Electron. Appl.*, 2011, pp. 1–9.

[9] K. Atallah, D. Howe, P. Mellor, and D. Stone, "Rotor loss in permanent magnet brushless ac machines," in *Proc. IEEE Int. Electr. Mach. Drives Conf. (IEMDC)*, 1999, pp. 60–62.

[10] L. J. Wu, Z. Q. Zhu, D. Staton, M. Popescu, and D. Hawkins, "Analytical model of eddy current loss in windings of permanent-magnet machines accounting for load," *IEEE Trans. Magn.*, vol. 48, no. 7, pp. 2138–2151, 2012.

[11] Z. Zhu, K. Ng, N. Schofield, and D. Howe, "Analytical prediction of rotor eddy current loss in brushless machines equipped with surface-mounted permanent magnets. ii. accounting for eddy current reaction field," in *Proc. Int. Conf. Electr. Mach. Syst. (ICEMS)*, vol. 2, 2001, pp. 810–813 vol.2.

[12] W. Tong, L. Sun, S. Wu, M. Hou, and R. Tang, "Analytical model and experimental verification of permanent magnet eddy current loss in permanent magnet machines with nonconcentric magnetic poles," *IEEE Trans. Ind. Electron.*, vol. 69, no. 9, pp. 8815–8824, 2022.

[13] Z. Zhang, Z. Deng, C. Gu, Q. Sun, C. Peng, and G. Pang, "Reduction of rotor harmonic eddy-current loss of high-speed PM BLDC motors by using a split-phase winding method," *IEEE Trans. Energy Convers.*, vol. 34, no. 3, pp. 1593–1602, 2019.

[14] F. Dubas and A. Rahideh, "Two-dimensional analytical permanent-magnet eddy-current loss calculations in slotless PMSM equipped with surface-inset magnets," *IEEE Trans. Magn.*, vol. 50, no. 3, pp. 54–73, 2014.

[15] F. Martin, M. E.-H. Zaïm, A. Tounzi, and N. Bernard, "Improved analytical determination of eddy current losses in surface mounted permanent magnets of synchronous machine," *IEEE Trans. Magn.*, vol. 50, no. 6, pp. 1–9, 2014.

[16] M. Mirzaei, A. Binder, B. Funieru, and M. Susic, "Analytical calculations of induced eddy currents losses in the magnets of surface

mounted PM machines with consideration of circumferential and axial segmentation effects," *IEEE Trans. Magn.*, vol. 48, no. 12, pp. 4831–4841, 2012.

[17] W.-Y. Huang, A. Bettayeb, R. Kaczmarek, and J.-C. Vannier, "Optimization of magnet segmentation for reduction of eddy-current losses in permanent magnet synchronous machine," *IEEE Trans. Energy Convers.*, vol. 25, no. 2, pp. 381–387, 2010.

[18] M. Merdzan, A. Borisavljevic, and E. A. Lomonova, "Modeling the influence of commutation in voltage source inverters on rotor losses of permanent magnet machines," in *Proc. Eur. Conf. Power Electron. Appl.*, 2014, pp. 1–10.

[19] Z. Song, C. Liu, K. Feng, H. Zhao, and J. Yu, "Field prediction and validation of a slotless segmented-halbach permanent magnet synchronous machine for more electric aircraft," *IEEE Trans. Transport. Electrific.*, pp. 1–1, 2020.

[20] A. Tessarolo, L. Branz, and C. Bruzzese, "A compact analytical expression for the load torque in surface permanent-magnet machines with slotless stator design," in *Proc. IEEE Workshop Electr. Mach. Des. Control Diagn. (WEMDCD)*, 2013, pp. 8–17.

[21] D. G. Holmes and T. A. Lipo, *Modulation of ThreePhase Voltage Source Inverters*, 2003, pp. 215–258.

[22] M. J.F., E. M.G., and M. J.M.D., "Theoretical spectra of space-vector-modulated waveforms," *IEE Proc.: Electr. Power Appl.*, vol. 145, pp. 17–24(7), January 1998.

[23] K. Zhou and D. Wang, "Relationship between space-vector modulation and three-phase carrier-based pwm: a comprehensive analysis [three-phase inverters]," *IEEE Trans. Ind. Electron.*, vol. 49, no. 1, pp. 186–196, 2002.

[24] G. Grandi and J. Loncarski, "Evaluation of current ripple amplitude in three-phase PWM voltage source inverters," in *Proc. IEEE Int. Conf. Workshop Compat. Power Electron.*, 2013, pp. 156–161.

[25] D. Jiang and F. Wang, "Study of analytical current ripple of three-phase PWM converter," in *Proc. Annu. IEEE Appl. Power Electron. Conf. Expo. (APEC)*, 2012, pp. 1568–1575.

[26] M. Leandro, "Induced PM eddy current model in slotless pm machines," https://www.codeocean.com/, 10 2022.

[27] J. Moynihan, M. Egan, and J. Murphy, "Theoretical spectra of space-vector-modulated waveforms," *IEE Proc.: Electr. Power Appl.*, vol. 145, no. 1, pp. 17–24, 1998.

[28] H. Soltani, P. Davari, F. Zare, P. C. Loh, and F. Blaabjerg, "Characterization of input current interharmonics in adjustable speed drives," *IEEE Trans. Power Electron.*, vol. 32, no. 11, pp. 8632–8643, 2017.

[29] W. Chen, B. Li, D. Xu, and L. Cai, "A dead-time compensation method for voltage source inverters," in *2019 22nd International Conference on Electrical Machines and Systems (ICEMS)*, 2019, pp. 1–6.

[30] A. Rahideh, M. Mardaneh, and T. Korakianitis, "Analytical 2-d calculations of torque, inductance, and back-emf for brushless slotless machines with surface inset magnets," *IEEE Trans. Magn.*, vol. 49, no. 8, pp. 4873–4884, 2013.

[31] A. Vahaj, A. Rahideh, H. Moayed-Jahromi, and A. Ghaffari, "Exact two-dimensional analytical calculations for magnetic field, electromagnetic torque, umf, back-emf, and inductance of outer rotor surface inset permanent magnet machines," *Math. Comput. Appl.*, vol. 24, no. 1, 2019.

[32] Z. Zhu, K. Ng, N. Schofield, and D. Howe, "Improved analytical modelling of rotor eddy current loss in brushless machines equipped with surface-mounted permanent magnets," *IEE Proc.: Electr. Power Appl.*, vol. 151, no. 6, pp. 641–650, 2004.

[33] P.-D. Pfister, X. Yin, and Y. Fang, "Slotted permanent-magnet machines: General analytical model of magnetic fields, torque, eddy currents, and permanent-magnet power losses including the diffusion effect," *IEEE Trans. Magn.*, vol. 52, no. 5, pp. 1–13, 2016.

[34] Z. Zhang, Z. Deng, Q. Sun, C. Peng, Y. Gu, and G. Pang, "Analytical modeling and experimental validation of rotor harmonic eddy-current loss in high-speed surface-mounted permanent magnet motors," *IEEE Trans. Magn.*, vol. 55, no. 2, pp. 1–11, 2019.

[35] P.-D. Pfister and Y. Perriard, "Slotless permanent-magnet machines: General analytical magnetic field calculation," *IEEE Trans. Magn.*, vol. 47, no. 6, pp. 1739–1752, 2011.

[36] P. Holoborodko, "Accuracy of bessel functions in matlab."

[37] M. Leandro, "Analytical-Field-Formulations-for-Slotless-Machines," 2 2023. [Online]. Available: https://github.com/Matteo-Lea/Analytical-Field-Formulations-for-Slotless-Machines

Matteo Leandro received the M.Sc. degree in electrical energy engineering from the University of Padova, Padua, Italy, in 2019. He is currently a PhD candidate at Department of Electric Power Engineering, Norwegian University of Science and Technology (NTNU), Trondheim, Norway. His current research interests include analytical formulations for electrical machine analysis, slotless machines and multiphysics. He is cooperating closely with Alva Industries AS, Trondheim, where his research is applied to analytical modeling and digital twin development of electric drives using slotless machines. The aim is to move towards development of lightweight coreless machines for aerial propulsion systems. Mr. Leandro regularly serves as a reviewer in several IEEE journals and conferences.

Jonas Kristiansen Nøland (S'14-M'17-SM'22) was born in Drammen, Norway, in 1988. He received the M.Sc. degree in electric power engineering from the Chalmers University of Technology, Gothenburg, Sweden, in 2013, and the Ph.D. degree in engineering physics from Uppsala University, Uppsala, Sweden, in 2017. Since 2018, he has been an Associate Professor with the Department of Electric Power Engineering, Norwegian University of Science and Technology. He is also currently an Associate Professor II with the Department of Electrical engineering, Information Technology, and Cybernetics at the University of South-Eastern Norway (USN) and the communication manager of the hydropower systems project SysOpt supported by The Research Council of Norway (RCN). His current research interests include excitation systems, hydrogenerators, large AC machines, and enhancing their utilization. Dr. Nøland serves as an Associate Editor for the IEEE TRANSACTIONS ON ENERGY CONVERSION and the IEEE TRANSACTIONS ON INDUSTRIAL ELECTRONICS, and as the Chair of the IEEE Power and Energy Society (PES) Norwegian Chapter since 2022.